Model Predictive Control based on Dynamic Voltage Vectors for Six-phase Induction Machines

Juan J. Aciego[1], I. Gonzalez-Prieto[1], M. J. Duran[1], M. Bermudez[2], P. Salas-Biedma[1]

***Abstract*— Model predictive control (MPC) has been recently suggested as an interesting alternative for the regulation of multiphase electric drives because it easily exploits the inherent advantages of multiphase machines. However, standard MPC applies a single switching state during the whole sampling period, inevitably leading to an undesired x-y voltage production. Consequently, its performance can be highly degraded when the stator leakage inductance is low. This shortcoming has been however mitigated in recent works with the implementation of virtual/synthetic voltage vectors (VVs) in MPC strategies. Their implementation reduces the phase current harmonic distortion since the average x-y voltage production becomes null. Nevertheless, VVs have a static nature because they are generally estimated offline, and this implies that the flux/torque regulation is suboptimal. Moreover, these static VVs also present some limitations from the point of view of the DC-link voltage exploitation. Based on these previous limitations, this work proposes the implementation of dynamic virtual voltage vectors (DVVs), where VVs are created online within the MPC strategy. This new concept provides an online optimization of the output voltage production depending on the operating point, resulting in an enhanced flux/torque regulation and a better use of the DC-link voltage. Experimental results have been employed to assess the goodness of the proposed MPC based on DVVs.**

***Index Terms*— Dynamic virtual voltage vectors, model predictive control, six-phase induction machines.**

I. Introduction

Finite-control-set model predictive control (FCS-MPC) has been widely studied for the current regulation of multiphase machines [1-4]. Standard field oriented control (FOC) performs the current regulation using proportional-integral (PI) controllers and a pulse width modulation (PWM) stage [5-7], whereas the MPC strategy directly selects the optimal switching state and applies it during the whole sampling period. In this sense MPC is closer to Direct Torque Control (DTC) [2,5,8-9], obtaining variable switching frequency and fast dynamic response in both techniques. Originally suggested for three-phase electric drives, the lack of modulation resulted in higher current ripple but, at the same time, the predictive approach provided better dynamic response and high flexibility [10]. Initial attempts to extend the MPC strategy to multiphase machines followed the same procedure, but they used a cost function with the secondary x-y currents that are inherent to multiphase systems [11]. Unfortunately, the performance of MPC was much poorer than in three-phase drives for the simple reason that a single switching state simultaneously maps into the main (α-β) and secondary (x-y) planes. Hence, the production of non-null average x-y voltage became inevitable, leading to high parasitic currents when the stator leakage inductance is reasonably low [12]. Although flux/torque control could be performed satisfactorily in distributed-winding multiphase induction machines (IMs), the appearance of high x-y currents spoiled the current quality and efficiency. Even though the x-y currents can be a source of additional stator copper losses, these additional degrees of freedom provide multiphase machines with well-known advantages over their three-phase counterparts [1-2,12]. The fault-tolerance against open-phase faults is one of the most claimed ones [13-14], but some recent investigations have shown other innovative uses of the additional degrees of freedom. Shifting the active and reactive power between three-phase windings [15], regulating the voltage of the DC-link midpoint in series-connected VSCs [16], enhancing the braking capability using the stator as a braking resistor [17] and using improved on-board chargers for electrical vehicles [18] are some examples.

Aiming to solve the aforementioned limitation with regard to the x-y current regulation, the concept of virtual/synthetic voltage vectors was introduced in [19] for the improvement of direct torque control (DTC) scheme in multiphase drives. In essence, VVs are a combination of several switching states in such a manner that the average x-y voltage production becomes null. Consequently, the application of VVs simplifies the control structure and guarantees low x-y currents in reasonably well-balanced multiphase IMs. The inclusion of VVs into DTC-based multiphase drives was also conducted in [20-24], and later on they were also adopted together with MPC strategies [25-33]. The concept was also extended from five-phase to six- and nine-phase drives [20-21, 23-24, 27, 29-33]. Whereas the determination of the most adequate switching states to form the VV becomes more complex as the number of phases grows, the concept is mostly the same for different multiphase systems, i.e., minimizing the x-y voltage production and, at the same time, maximizing the α-β voltage generation [33]. Different versions of MPC suggest the use of a single VV [19-23, 31, 33], the joint use of a VV and the zero vector [25-30] or the combination of several VVs [32]. Nevertheless, the VVs that have been used in all cases have a static nature because they are determined offline (e.g., in [31] the large and medium-large vectors are applied during 73% and 27% of the sampling period, respectively). In other words, the time of application of each switching state within the VV is fixed in advanced, and this predefined combination is later on used in real-time control. Regardless of how VVs are combined and independently from

This work was supported by the Spanish Ministry of Science, Innovation and Universities under Project RTI2018-096151-B-100.

Juan J. Aciego, I. Gonzalez-Prieto, M.J. Duran and P. Salas-Biedma are with the Department of Electrical Engineering at the University of Malaga, Spain, e-mail: juanjoseaciego@uma.es, ignaciogp87@gmail.com, mjduran@uma.es and psbiedma@uma.es

M. Bermudez is with the Department of Electrical Engineering at the University of Huelva, Spain, email: mariobermg@gmail.com.

the control approach and number of phases, none of the existing works in literature have tried to generate the VVs dynamically, i.e., adjusting the selection of switching states and their proportion in real time within the MPC strategy.

In spite of the better performance of VV-MPC compare to standard strategies, there are two main shortcomings that are inherent to the static nature of the VVs:

S1. There is no flexibility for the control designer to promote the current tracking in either of the α-β or x-y planes.

S2. The voltage production is confined to specific discrete values and consequently the output voltage cannot be adapted to each operating point.

Issue S1 cannot be solved in VV-MPC because the x-y control is performed in open-loop mode, hence the cost function solely depends on the α-β current tracking [34]. Similarly, the machine equations in the secondary plane are completely omitted since there is no need to predict the x-y currents. In distributed-winding machines the α-β currents are responsible for the flux/torque production, whereas the x-y currents are just a source of stator copper losses [12]. Consequently, the dynamic performance can be improved with a higher accuracy in the α-β current tracking, whereas the copper losses can be mitigated if the ripple of the x-y currents is lower. In standard MPC the designer can search for a tradeoff between both issues just adjusting the weighting factors in the cost function [35-36]. It follows that the inclusion of VVs results in a loss of flexibility to promote either the flux/torque tracking or the efficiency for each specific application.

With regard to issue S2, in six-phase machines there are only 12 VVs that are formed with large vectors (applied during 73% of the sampling period) and medium-large vectors (applied the remaining 27%) [31]. Regardless of the voltage that is required at each sampling period, the VV-MPC can only apply one of the 12 predefined VVs or the zero vector. Although some operating points would better require the combination of other vectors (e.g., large & large or large & zero vectors when voltage requirements are high and low, respectively) or other times of application (different from 73% and 27%), the static nature of the VVs does not provide flexibility to change neither the switching state nor their times of application. For this reason, the implementation of VVs in MPC strategies is inherently suboptimal.

On the basis of the aforementioned shortcomings, this works advances one step beyond by dynamically determining the VVs in real time within the MPC loop. At each sampling time, the proposed algorithm will select online both the switching states and their times of application with no predefined assumptions (except for the exclusion of the small vectors). Consequently, the VVs are constantly changing to search for the optimal combination at each sampling time, and for this reason they will be referred from now on as dynamic voltage vectors (DVVs). Both the vectors that are selected to form the VV and their proportion can be adjusted according to the operating point of the multiphase drive. Furthermore, the construction of the VV will also depend on the designer specifications: by adjusting the weighting factors in the proposed DVV-MPC it is possible to promote the current tracking in either α-β or x-y planes. In few words, the DVVs regain the design flexibility of standard MPC with the capability to further reduce the x-y currents compared to VV-MPC.

The main disadvantage of the proposed DVV-MPC is the increased computational cost. However, S1 and S2 shortcomings are overcome, thus providing a higher flexibility and current quality. The approach is also novel in essence because all previous works are based on static VVs. This work aims to be a proof-of-concept about the interest of using an online optimization to form the VV as a means to improve the MPC performance.

The paper is structured as follows: Section II reviews some generalities of six-phase IM drives. Section III describes the model predictive control using static virtual voltage vectors. Section IV details the proposed procedure to determine the dynamic voltage vectors that are included within the MPC strategy. Section V provides experimental results that compare the performance of static and dynamic VVs. Finally, Section VI summarizes the main conclusions obtained.

II. Generalities of Six-Phase IM Drives

A. Topology description

The system employed in this work includes an asymmetrical six-phase IM and a six-phase voltage source converter (VSC) obtained from two parallel three-phase two-level inverters (Fig. 1). Vector $[S]$=$\{S_{a1}, S_{b1}, S_{c1}, S_{a2}, S_{b2}, S_{c2}\}$ defines the different VSC leg switching states, being S_{ij}=0 if the lower switch is ON and the upper switch is OFF and 1 otherwise. Thereby, $[S]$ allows expressing the $2^6 = 64$ available VSC switching states in a single vector using a binary coding. To obtain stator phase voltages, it is necessary to employ the vector $[S]$, the DC-link voltage (V_{dc}) and the transformation matrix from leg to phase variables as follows:

$$\begin{bmatrix} v_{as1} \\ v_{bs1} \\ v_{cs1} \\ v_{as2} \\ v_{bs2} \\ v_{cs2} \end{bmatrix} = \frac{V_{dc}}{3} \begin{bmatrix} 2 & -1 & -1 & 0 & 0 & 0 \\ -1 & 2 & -1 & 0 & 0 & 0 \\ -1 & -1 & 2 & 0 & 0 & 0 \\ 0 & 0 & 0 & 2 & -1 & -1 \\ 0 & 0 & 0 & -1 & 2 & -1 \\ 0 & 0 & 0 & -1 & -1 & 2 \end{bmatrix} \cdot \begin{bmatrix} S_{a1} \\ S_{b1} \\ S_{c1} \\ S_{a2} \\ S_{b2} \\ S_{c2} \end{bmatrix} \quad (1)$$

In order to simplify control strategies, vector space decomposition (VSD) provides simpler means for the model-based regulation of multiphase drives. Hence, applying the amplitude invariant decoupling Clarke transformation, it is

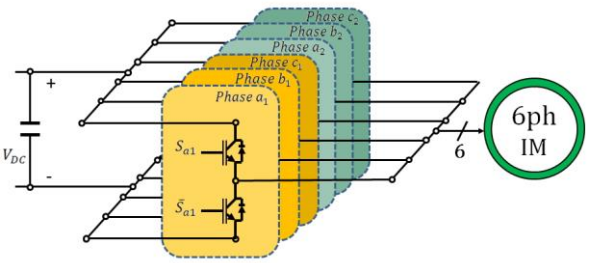

Fig. 1. Scheme of a six-phase IM drive.

possible to obtain the vector space decomposed voltages (2):

$$[T]=\frac{1}{3}\begin{bmatrix}1 & -1/2 & -1/2 & \sqrt{3}/2 & -\sqrt{3}/2 & 0\\ 0 & \sqrt{3}/2 & -\sqrt{3}/2 & 1/2 & 1/2 & -1\\ 1 & -1/2 & -1/2 & -\sqrt{3}/2 & \sqrt{3}/2 & 0\\ 0 & -\sqrt{3}/2 & \sqrt{3}/2 & 1/2 & 1/2 & -1\\ 1 & 1 & 1 & 0 & 0 & 0\\ 0 & 0 & 0 & 1 & 1 & 1\end{bmatrix} \quad (2)$$

$$\left[v_{\alpha s}, v_{\beta s}, v_{xs}, v_{ys}, v_{0+}, v_{0-}\right]^T = [T]\cdot\left[v_{a1}, v_{b1}, v_{c1}, v_{a2}, v_{b2}, v_{c2}\right]^T$$

Using standard assumptions [37], the model of this multiphase machine can be transformed into VSD variables, by employing (2).

$$\begin{aligned} v_{\alpha s} &= \left(R_s + L_s\frac{d}{dt}\right)i_{\alpha s} + M\frac{di_{\alpha r}}{dt}\\ v_{\beta s} &= \left(R_s + L_s\frac{d}{dt}\right)i_{\beta s} + M\frac{di_{\beta r}}{dt}\\ v_{xs} &= \left(R_s + L_{ls}\frac{d}{dt}\right)i_{xs}\\ v_{ys} &= \left(R_s + L_{ls}\frac{d}{dt}\right)i_{ys}\\ 0 &= \left(R_r + L_r\frac{d}{dt}\right)i_{\alpha r} + M\frac{di_{\alpha s}}{dt} + \omega_r L_r i_{\beta r} + \omega_r M i_{\beta s}\\ 0 &= \left(R_r + L_r\frac{d}{dt}\right)i_{\beta r} + M\frac{di_{\beta s}}{dt} - \omega_r L_r i_{\alpha r} - \omega_r M i_{\alpha s}\\ T_e &= 3pM(i_{\beta r}i_{\alpha s} - i_{\alpha r}i_{\beta s}) \end{aligned} \quad (3)$$

where $L_s = L_{ls} + M$, $L_r = L_{lr} + M$, $M = 3\cdot L_m$, and $\omega_r = p\cdot\omega_m$, being p and ω_m the pole pairs number and the mechanical speed, respectively. In addition, indices s and r denote stator and rotor variables and subscripts l and m denote leakage and magnetizing inductance, respectively.

The zero-sequence currents (i_{0+}, i_{0-}) are omitted from this analysis because the machine is configured with two isolated neutral points and, therefore, these currents cannot flow. Conversely, α-β and x-y currents are responsible for the flux/torque generation and the stator copper losses, respectively. For this reason, these subspaces must be properly regulated in order to provide a suitable dynamic performance and satisfactory efficiency. On the other hand, this work assumes a distributed-winding IM as well as negligible spatial harmonics.

The control stage typically requires employing d-q components in a rotating reference frame to decouple flux and torque regulation. For this purpose, the transformation from stationary reference frame (3) to rotating frame via Park transformation can be used (4), where θ_s is the angle of rotor flux [12].

$$[D]=\begin{bmatrix}cos\theta_s & sin\theta_s\\ -sin\theta_s & cos\theta_s\end{bmatrix} \quad \left[i_{ds}, i_{qs}\right]^T = [D]\cdot\left[i_{\alpha s}, i_{\beta s}\right]^T \quad (4)$$

B. Voltage vectors in six-phase VSCs.

As previously exposed, each of the $2^6 = 64$ available voltage vectors in a six-phase machine is mapped in both α-β and x-y subspaces. Consequently, fulfilling simultaneously the α-β and x-y requirements is not possible if a single switching state is applied during the whole sampling period, as it occurs in standard MPC.

Analyzing the $2^6 = 64$ voltage vectors mapped in α-β and x-y subspaces, it is possible to classify them into small, medium, medium-large and large vectors according to their size in the α-β subspace. Note that medium-large vectors in α-β subspace result in medium-large vectors in x-y subspace, whereas large vectors in the main α-β plane correspond to small vectors in the secondary subspace, and vice versa [12]. Furthermore, medium-large and large vectors with a common direction in the α-β plane have opposite directions in the x-y subspace. This special localization of the voltage vectors has allowed the implementation of VVs in order to satisfy the α-β and x-y requirements for MPC and DTC strategies in multiphase machines [19-21, 31-32].

III. Model-based Predictive Control employing Virtual Voltage Vectors

A. Standard Model Predictive Control in six-phase drives

Standard FCS-MPC strategies iteratively evaluate all available switching states of the VSC (64 in a dual three-phase two-level VSC) every sampling time, and consequently this implies a high computational burden. MPC allows the tracking of the reference stator currents ($i^*_{\alpha\beta xy}$) using a predictive IM model (using the standard Euler discretization) that predicts the future values of stator currents ($\hat{\imath}_{\alpha\beta xy}$) [6]. Multiphase MPC-based schemes typically include an outer speed loop with a PI controller and inner current loops that are implemented with a model predictive approach. The speed loop provides the q-current reference whereas the d-current reference is assumed to be constant and proportional to the rated magnetic flux. For regulation purposes the d-q reference currents are expressed as α-β components via the inverse Park transformation [2,12].

The optimization process is performed by exhaustive search over the different switching states. The comparison between the predicted and the reference stator currents allows determining the optimal signal gating (S_{opt}) by minimizing a cost function J_v that takes into account the error in the α-β and x-y currents as follows:

$$J_v = e_\alpha^2 + e_\beta^2 + K_{xy}\cdot\left(e_x^2 + e_y^2\right) \quad (5)$$

where:

$$\begin{aligned} e_\alpha &= (i^*_{\alpha s} - \hat{\imath}_{\alpha s}) \qquad e_x = (i^*_{xs} - \hat{\imath}_{xs})\\ e_\beta &= (i^*_{\beta s} - \hat{\imath}_{\beta s}) \qquad e_y = (i^*_{ys} - \hat{\imath}_{ys}) \end{aligned} \quad (6)$$

The K_{xy} coefficient is the weighting factor for the x-y currents error term in the cost function. In distributed-winding machines the reference values of the x-y currents are set to zero in order to reduce the stator copper losses. However, as previously described, the active voltage vectors are simultaneously mapped into α-β and x-y planes, therefore it is impossible to satisfy α-β and x-y requirements with the application of a single switching state during the sampling period. This fact can considerably degrade the MPC performance for low values of the stator leakage inductance [12].

B. Model Predictive Control using Virtual Voltage Vectors (VV-MPC)

In order to minimize the x-y harmonic currents that appear in standard MPC, voltage vectors can be replaced by virtual/synthetic voltage vectors that ensure a null average x-y voltage production. Taking advantage of the spatial localization of the voltage vectors in α-β and x-y subspaces, VVs are synthesized applying one medium-large and one large voltage vector [31]. Consequently, 12 active VVs and a single null vector provide the new available voltage states. Each voltage vector from the pair must be applied with a different application time during the sampling period in order to generate zero average voltage in the x-y subspace. For the proposed topology, the large vector application time is $t_1 = 0.73 \cdot T_s$ and medium-large vector application time is $t_2 = 0.27 \cdot T_s$, being T_s the sampling time. Following the aforementioned statement, a general expression for the VV can be defined:

$$VV_i = t_1 \cdot V_{large} + t_2 \cdot V_{medium-large} \quad (7)$$

The regulation of the x-y currents is directly carried out in open-loop mode with the implementation of VV-MPC. Since the predictive algorithm does no longer need to include the secondary components, it is possible to reduce the predictive model. Furthermore, x-y components are also absent in the cost function of VV-MPC:

$$J_{VV} = e_\alpha^2 + e_\beta^2 \quad (8)$$

To sum up, the inclusion of VVs in the MPC scheme highly mitigates the harmonic distortion and, at the same time, simplifies the control because the x-y currents are regulated indirectly with the implementation of the VVs. Moreover, a reduced model predictive control and a cost function with a lower number of terms can be implemented, reducing the computational cost of MPC.

IV. Proposed DVV-MPC Control Algorithm

The proposed control algorithm introduces an online method to generate VVs that can be dynamically adjusted at different operating points. Aiming to overcome S1 (lack of flexibility) and S2 (discrete nature of the voltage vectors) shortcomings, the dynamic voltage vectors are designed to achieve an enhanced α-β currents tracking with reduced stator copper losses. For this purpose, the algorithm that calculates the DVV uses three stages to determine both the two optimal switching states and their respective application times. The capability of the DVV algorithm to modify the times of application allows covering in a continuous manner the whole voltage range, this being opposed to the discrete nature of static VVs that use a fixed proportion. Furthermore, the DVV algorithm regains the capability of standard MPC to tune the weighting factors to either promote α-β or x-y currents, which is inexistent in static VVs. To sum up, the proposed regulation strategy searches the dynamic combination of vectors pairs and the corresponding application times in order to obtain improved current quality and efficiency. Since both DVV-MPC and VV-MPC strategies follow a predictive-based approach, their performance is expected to have some parameter dependence. A detailed study on the sensitivity of predictive controllers to parameter variation can be found in [38]. In any case, the main difference between VV-MPC and DVV-MPC is not related to the model or parameters, but to the procedure to select the voltage vectors and times of application (offline in VVs and online in DVVs).

As an initial step in the DVV algorithm, it is analyzed if some of the $2^6 = 64$ switching states of the six-phase VSC can be discarded in advance to alleviate the computational burden of the iterative MPC process. For this purpose, it is worth noting the existence of 12 duplicate states that provide the same output voltage. Taking advantage of this redundancy, these 12 states are eliminated from the analysis in order to ease the real-time implementation. In addition, some voltage vectors have a marginal contribution in the α-β subspace and a high magnitude in the x-y plane. This implies that the capability of these voltage vectors to produce flux/torque is very limited and, at the same time, large stator copper losses are expected. Since the aim of the voltage vectors is to drive the machine creating proper flux/torque with minimum copper losses, such vectors should not be considered in the DVV algorithm. For such purpose, the relative value of the voltage production in α-β and x-y planes of the 4 aforementioned groups of voltage vectors: large, medium-large, medium and small voltage vectors (termed C_L, C_{ML}, C_M and C_S, respectively) is quantified in Table I, using the following ratio:

$$R_{\alpha\beta} = {|v_{\alpha\beta}|}/{|v_{xy}|} \quad (9)$$

where $|v_{\alpha\beta}|$ and $|v_{xy}|$ are the voltage vector modulus in α-β and x-y planes, respectively.

Note that, in order to illustrate the goodness of the different voltage vector groups, a percentage of the $R_{\alpha\beta}$ ratio taking C_L as base value is also included in Table I.

As shown in Table I, the ratio $R_{\alpha\beta}$ of the group C_S (i.e., small vectors in the α-β subspace which are mapped into large vectors in the x-y plane) is extremely low (8%). This indicates that the 12 small vectors grouped in C_S are not adequate to efficiently generate flux and torque and, for this reason, they are also omitted from the analysis. To sum up, duplicated medium vectors and all small vectors are discarded in advance to improve the flux/torque production and reduce the computational burden. Finally, only one null vector is used among the four available in a six-phase VSC. After this preliminary analysis, only a subset of 37 switching states (see Fig. 2) will be considered in the proposed algorithm. The DVV-MPC scheme is shown in Fig. 3, which consists of three stages that are detailed next.

TABLE I
AMPLITUDE AND CONTRIBUTION RATIO OF THE VOLTAGE VECTORS IN EACH SUBSPACE GROUPED C_L TO C_S NORMALIZED WITH V_{DC}

Group	C_L	C_{ML}	C_M	C_S
$\|v_{\alpha\beta}\| \cdot 100$	64	47	33	17
$\|v_{xy}\| \cdot 100$	17	47	33	64
$R_{\alpha\beta}$	3.8	1	1	0.3
%	100	27	27	8

A. *Stage 1: preselection of the four best voltage vectors*

This first step consists in implementing a standard MPC with a finite control set of 37 possible vectors (Fig. 2), where the four best voltage vectors are selected. Measured currents and mechanical speed are used as inputs in the predictive model. The set of voltage vectors is iterated 37 times, generating predictions of α-β and x-y currents. A predefined cost function J_{s1} evaluates the drive performance and 37 values of cost function (J_{s1}^{1} to J_{s1}^{37}, in descending order of the provided error) are obtained using the following expression:

$$J_{s1} = (e_\alpha^2 + e_\beta{}^2) + K_{xy1} \cdot (e_x{}^2 + e_y{}^2) \quad (10)$$

Note that e_α, e_β, e_x and e_y in (10) are the α-β and x-y currents errors previously defined in (6). On the other hand, the coefficient K_{xy1} is the weighting factor for the x-y currents error term in the cost function, and it is determined by the designer in order to satisfy the control objectives and system features. Considering that it is impossible to serve the regulation objectives in a sampling period with a single voltage vector [12], it is necessary to assume a tradeoff between the flux/torque regulation and the harmonic distortion attending to K_{xy1}.

The lower values of J_{s1} are selected because they provide a lower current tracking error. Therefore, the optimal voltage vector (V_1^{sel}) and the following three best ones (V_2^{sel}, V_3^{sel} and V_4^{sel}), corresponding to J_{s1}^1, J_{s1}^2, J_{s1}^3 and J_{s1}^4 cost function values, are the stage 1 outputs. These four preselected voltage vectors will be adequately combined in the following stages.

B. *Stage 2: selection of the optimum pair of voltage vectors*

This stage provides the best couple of voltage vectors to compose the DVV. This pair of voltage vectors (V_1^{opt} and V_2^{opt}) is selected among the four preselected voltage vectors in stage 1 (V_1^{sel},V_2^{sel}, V_3^{sel} and V_4^{sel}). Even though V_1^{sel} and V_2^{sel} are individually the best two vectors, they might not be the best pair if they are not compatible (i.e., their x-y components do not cancel). In stage 2, the optimal couple of voltage vectors is obtained using a new cost function J_{s2} presented in (11), combining the cost function values of stage 1 (first two terms in (11)) and the x-y voltages of the selected voltage vectors (last term in (11)). This last term of the proposed cost function promotes pairs of vectors whose x-y components have opposite directions. Since the cost function (J_{s2}) is evaluated for each pair of preselected voltage vectors, six cost function values ($\binom{4}{2} = 6$) are calculated in this stage.

$$J_{s2} = J_{s1}^i + J_{s1}^j + K_w \cdot \left[\left(v_x^i + v_x^j\right)^2 + \left(v_y^i + v_y^j\right)^2 \right] \quad (11)$$

J_{s1}^i and J_{s1}^j: cost functions corresponding to preselected voltage vectors i and j in stage 1.
K_w: weighting factor that penalizes the copper losses (see values in Table IV).
v_x^i and v_x^j: x-component of the preselected voltage vectors i and j in stage 1.
v_y^i and v_y^j: y-component of the preselected voltage vectors i and j in stage 1.

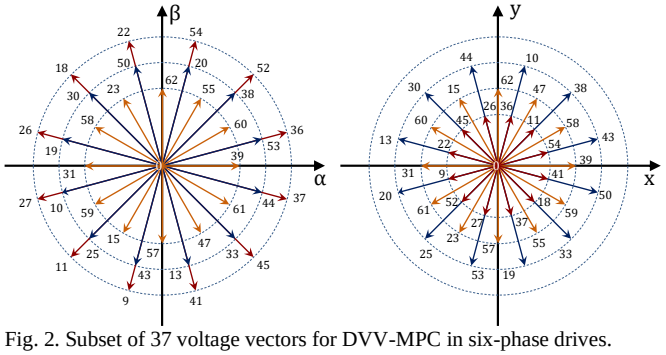

Fig. 2. Subset of 37 voltage vectors for DVV-MPC in six-phase drives.

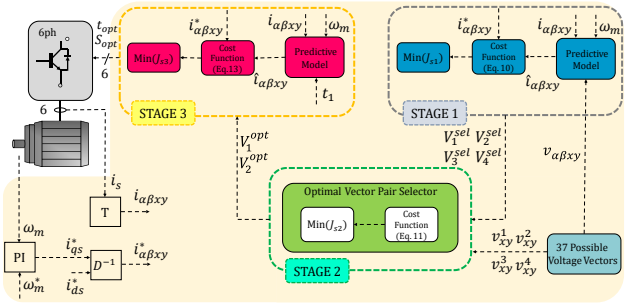

Fig. 3. DVV-MPC scheme for a six-phase IM drive

To detail the stage 2 performance, Table II exemplifies a case of study using 4 preselected voltage vectors from stage 1. This table shows the influence of the weighting factor K_w on the selection of the optimal couple of voltage vectors. For that purpose, two different values of K_w have been employed. As expected, low values of K_w do not give practical importance to the cancellation of x-y components (last term in (11)), hence the optimum vectors are the best two vectors from stage 1 (i.e., $V_1^{opt} = V_1^{sel} = 0$ and $V_2^{opt} = V_2^{sel} = 18$). Nevertheless, if the value of K_w is increased (up to 1 in Table II), then the best pair is $V_1^{opt} = V_2^{sel} = 18$ and $V_2^{opt} = V_3^{sel} = 22$ because voltage vectors 18 and 22 are mostly opposed in the x-y plane (see Fig. 2) and provide some degree of voltage cancellation.

In summary, stage 2 provides the optimal couple of voltage vectors to create the DVVs in accordance with the weighting factor K_w that can be adjusted by the control designer.

C. *Stage 3: determination of the optimal application times*

This last stage finally determines the application times for each of the optimum voltage vectors (V_1^{opt} and V_2^{opt}) from stage 2. These application times are expressed in per unit values taking T_s as base value, so V_1^{opt} is applied during t_{opt} and V_2^{opt} for the rest of the sampling period, $1 - t_{opt}$. The general expression of the proposed DVV is hence:

$$DVV_i = t_{opt} \cdot V_1^{opt} + (1 - t_{opt}) \cdot V_2^{opt} \quad (12)$$

In order to determine the optimal time to apply V_1^{opt}, an iterative search for different values of t_{opt} is computed. For such purpose, it is necessary to predict the α-β and x-y currents for each DVV_i and to evaluate the prediction using the cost function J_{s3} defined as follows:

$$J_{s3} = e_\alpha^2 + e_\beta^2 + K_{xy3} \cdot \left(e_x^2 + e_y^2\right) \quad (13)$$

Stage 3 is iterated 10 times, sweeping t_{opt} from 0.55 to 1 and obtaining 10 different cost function values with associated

dwell times (see Fig. 4). The lowest value of this proposed cost function allows selecting the optimal application time (t_{opt}) that define the DVV (V_1^{opt}, V_2^{opt}) to be applied to enhance the drive performance. Moreover, thanks to the fact that stage 3 uses a cost function including x-y currents, the inherent design flexibility of standard MPC is recovered in DVV-MPC.

V. Experimental Results

A. Test Bench

Experimental testing has been implemented using the test bench shown in Fig. 5. The six-phase drive is composed of an asymmetrical six-phase IM powered by conventional two-level three-phase VSCs (Semikron SKS22F modules). Table III shows the IM drive parameters obtained using AC time domain and stand still with inverter supply tests [39-40] and rated values employed in the experimental tests.

A single DC power supplies the VSCs and control actions are performed by a digital signal processor (TMS320F28335 from Texas Instruments, TI). The control unit is programmed using a JTAG and the TI proprietary software called Code Composer Studio. This control unit includes a data logger based on SD card for recording the experimental measurements. The data transmission between the digital signal processor and the SD card is based on SPI communication protocols. The current and speed measurements are taken with four hall-effect sensors (LEM LAH 25-NP) and a digital encoder (GHM510296R/2500), respectively. The six-phase IM is loaded coupling its shaft to a DC machine that acts as a generator. The armature of the DC machine is connected to a variable passive *R* load that dissipates the power and the load torque is consequently speed-dependent.

B. Experimental Results

The first test evaluates the current quality improvement that can be obtained thanks to the inclusion of DVVs into an FCS-MPC scheme. For that purpose, three different versions of MPC have been implemented: VV-MPC (Fig. 6, left column), DVV-MPC focused on x-y components (Fig. 6, middle column) and DVV-MPC focused on α-β components (Fig. 6, right column). The first three rows in Table IV show the weighting factors of the proposed MPC schemes for Test 1. Note that VV-MPC does not require any tuning since this MPC strategy employs a reduced model and a cost function without x-y components, while DVV-MPC focused on x-y components is set with higher values of the x-y weighting factors compared to the case of DVV-MPC focused on α-β components.

From the control point of view, the tracking of the reference speed is satisfactory in all three implemented strategies (see Fig. 6a). However, the current tracking performance is highly dependent on the selected control strategy and tuning of the weighting factors. As shown in Fig. 6e, the phase currents obtained with both DVV-MPC strategies present a lower ripple than the phase currents of VV-MPC. To quantify this improvement in the current quality, Table V presents some quality indices, including the stator current RMS value, total

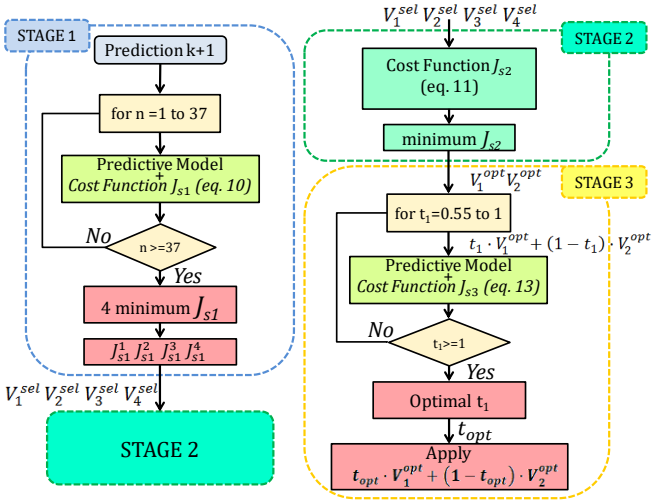

Fig. 4. Flowchart of the proposed DVV-MPC algorithm

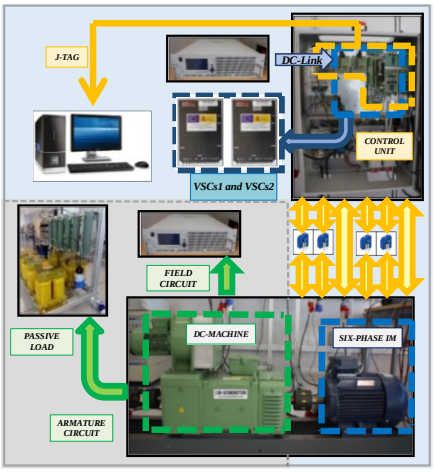

Fig. 5. Scheme of the test bench used for the experimental results.

.

TABLE II
SELECTION OF OPTIMAL PAIR OF VECTORS STARTING FROM 4 PRESELECTED VOLTAGE VECTORS IN STAGE 1 (CASE OF STUDY).

Preselected Voltage Vectors	Cost Function Values	Cost function J_{s2}	Weighting factor	Selected Optimal Pair of Vectors
$V_1^{sel} = 0$	$J_{s1}^1 = 0.0745$	$J_{s2} = J_{s1}^1 + J_{s1}^2 + K_w \cdot [(v_x^1 + v_x^2)^2 + (v_y^1 + v_y^2)^2]$ $J_{s2} = J_{s1}^1 + J_{s1}^3 + K_w \cdot [(v_x^1 + v_x^3)^2 + (v_y^1 + v_y^3)^2]$ $J_{s2} = J_{s1}^1 + J_{s1}^4 + K_w \cdot [(v_x^1 + v_x^4)^2 + (v_y^1 + v_y^4)^2]$ $J_{s2} = J_{s1}^2 + J_{s1}^3 + K_w \cdot [(v_x^2 + v_x^3)^2 + (v_y^2 + v_y^3)^2]$ $J_{s2} = J_{s1}^2 + J_{s1}^4 + K_w \cdot [(v_x^2 + v_x^4)^2 + (v_y^2 + v_y^4)^2]$ $J_{s2} = J_{s1}^3 + J_{s1}^4 + K_w \cdot [(v_x^3 + v_x^4)^2 + (v_y^3 + v_y^4)^2]$	K_w=1	$V_1^{opt} = 18$ $V_2^{opt} = 22$
$V_2^{sel} = 18$	$J_{s1}^2 = 1.2923$			
$V_3^{sel} = 22$	$J_{s1}^3 = 1.9731$		K_w=0.0005	$V_1^{opt} = 0$ $V_2^{opt} = 18$
$V_4^{sel} = 54$	$J_{s1}^4 = 2.0633$			

TABLE III
IM DRIVE PARAMETERS AND RATED VALUES IN EXPERIMENTAL TESTS

T_s (μs)	200
DC-link voltage (V)	300
i_{rated} (A)	6.5
f_{rated} (Hz)	50
V_{rated} (V)	220
n_m (rpm)	1000
R_s (Ω)	14.195
R_r (Ω)	2.05
L_m (mH)	420
L_{ls} (mH)	4.5
L_{lr} (mH)	55.12

harmonic distortion (THD) percentage in phase and α-β currents, and x-y current ripple (quantified as a standard deviation). Based on the results from Table V, the phase current THD is reduced by 33% with the inclusion of DVVs into an MPC scheme, compared to VV-MPC. Focusing on the x-y currents (Fig. 6d), DVV-MPC strategies decrease the ripple of these components, enhancing the performance of VV-MPC. As expected, DVV-MPC focused on x-y currents shows the best x-y current tracking, whereas DVV-MPC focused on α-β currents presents the lower THD percentage of components related with the flux/torque production (see Fig. 6c and Table V). DVV-MPC focused on α-β currents also achieves a better d-q current tracking performance (Fig. 6b). According to the results included in Test 1, DVVs allow improving the performance in the different subspaces, therefore achieving better phase current quality and reduced stator copper losses, as it can be observed from the current RMS values shown in Table V.

Test 2 shows the flexibility provided by DVV-MPC to regulate α-β and x-y currents when the reference speed is 400 rpm (Fig. 7a). On this occasion, three different settings of DVVs are employed to illustrate this capability of the proposed DVV-MPC (see the last three rows Table IV). The first configuration replays DVV-MPC focused on α-β currents (Fig. 7, left column). The second setting for DVV-MPC (Fig. 7, middle column) employs a similar configuration but the weighting factor K_w is reduced to 0.5 in order to stimulate the inclusion of the null vector in the pair of selected voltage vectors (DVV-MPC focused on null voltage vector). Finally, to optimize the flux/torque regulation, a new configuration of DVV-MPC (Fig. 7, right column) is also included in this second test, where the weighting factor K_{xy1} is defined with a null value (DVV-MPC focused on medium voltage vectors). Table VI presents again some quality indices to quantify the goodness of the proposed settings in DVV-MPC.

The histograms of the selected voltage vectors for each setting of DVV-MPC during the Test 2 are shown in Fig. 7f. The selection of $K_{xy1} = 0$ promotes the selection of medium voltage vectors (see the right column of Fig. 7f). However,

TABLE IV
WEIGHTING FACTORS FOR DIFFERENT SETTINGS IN EXPERIMENTAL TESTS

Test	MPC version	K_{xy1}	K_w	K_{xy3}
1	VV-MPC	-	-	-
1	DVV-MPC focused on x-y currents	0.7	1	0.60
1-2	DVV-MPC focused on α-β currents	0.3	1	0.25
2	DVV-MPC focused on null voltage vector	0.3	0.5	0.25
2	DVV-MPC focused on medium voltage vectors	0	1	0.40

TABLE V
TEST 1: PERFOMANCE QUALITY INDICES (VV-MPC VERSUS DVV-MPC)

MPC version	$THD_{ph}(\%)$	$RMS_{ph}(A)$	$THD_{\alpha\beta}(\%)$	σ_{xy}(A)
VV-MPC	46.9	1.46	17.25	0.66
DVV-MPC focused on x-y currents	31.6	1.44	20.40	0.37
DVV-MPC focused on α-β currents	31.2	1.44	15.20	0.44

as shown in Table VI, medium voltage vectors present a poor x-y performance and, therefore, the regulation of these components
is not satisfactory (Fig. 7d). Phase currents possess a high ripple (Fig. 7e) and the THD of the phase currents for this configuration is unacceptable (92%). To sum up, DVV-MPC focused on medium voltage vectors allows improving the flux/torque regulation, but provides a poor regulation of the x-y currents due to the low leakage inductance value. Although this setting is not valid for this IM, this configuration might be an interesting solution for IM with higher values of the leakage inductance.

On the other hand, the weighting factor relationship employed in DVV-MPC focused on null voltage vector promotes the selection of the zero voltage vector as an optimal voltage vector, as shown Fig. 7f. Since the zero voltage vector is also null in the x-y plane, an improved regulation of the x-y currents is obtained because this vector does not produce voltage in this secondary subspace. This is illustrated in the standard deviation of the x-y currents included in Table VI, showing that this DVV configuration provides the best x-y regulation. This DVV-MPC version also reduces the THD of the α-β currents, and therefore the phase currents also present an enhanced performance (see all these quality indices in Table VI). It can be observed that DVVs allow the designers to decide the best configuration of the weighting factors in order to satisfy their objectives, hence increasing the flexibility of the control strategy.

As a summary, it can be stated that DVV-MPC outperforms VV-MPC providing better current quality (verified in Test 1) and control flexibility (verified in Test 2).

The dynamic performance is verified in tests 3 (load rejection) and 4 (speed reversal). In Test 3 the machine is driven at 400 rpm when the load torque of 3 Nm is released at $t = 17\ s$, both in DVV-MPC and VV-MPC (left column and right column of Fig. 8, respectively). At this moment the reference q-current is decreased and the measured q-current closely

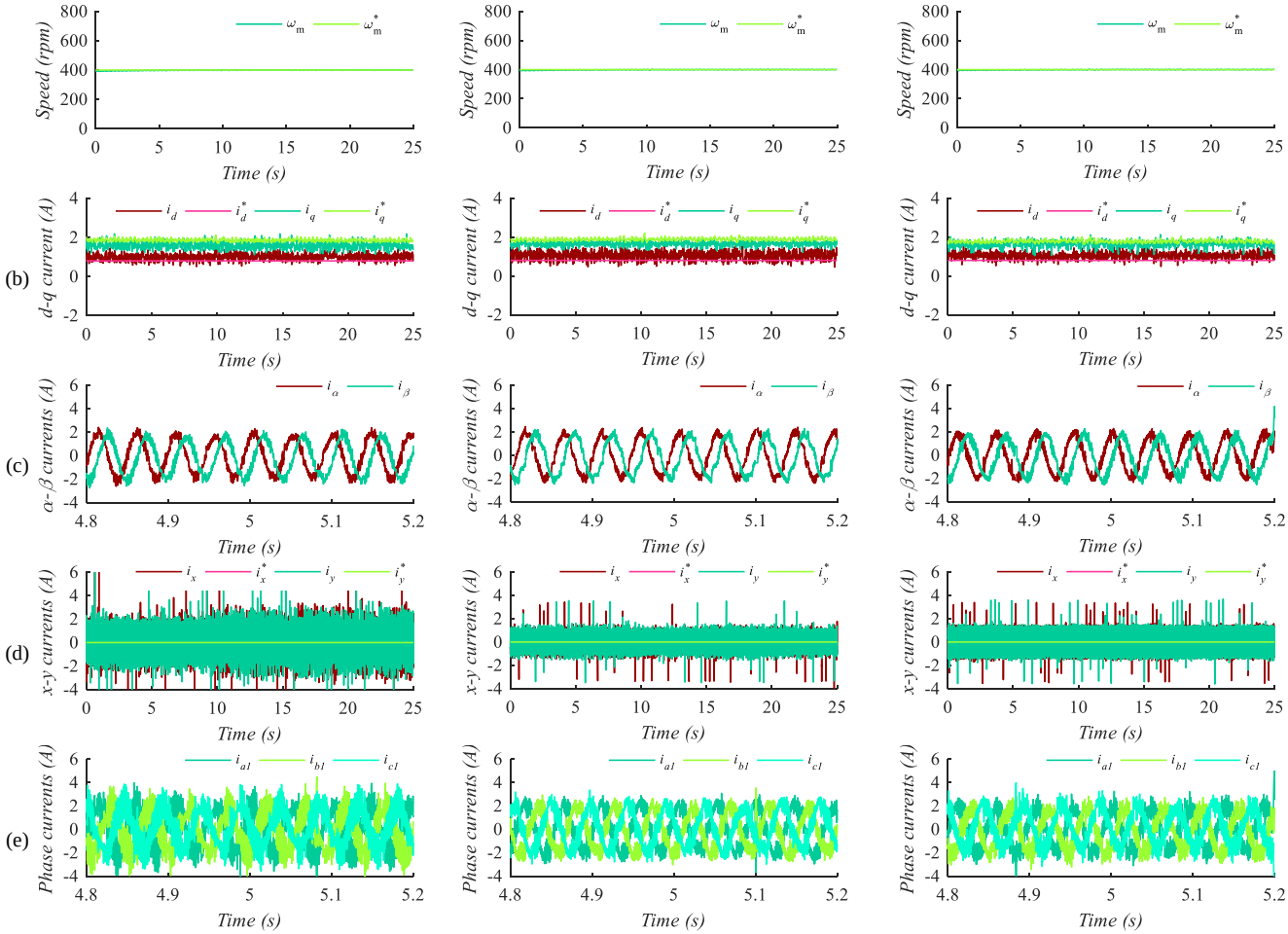

Fig. 6. Test 1: Steady-state performance of VV-MPC (left column), DVV-MPC focused on x-y currents (middle column) and DVV-MPC focused on α-β currents (right column). From top to bottom: (a) motor speed, (b) d-q currents, (c) α-β currents, (d) x-y currents and (e) phase currents set#1.

follows the reference (Fig. 8b) to maintain the speed at 400 rpm. The d-current is kept constant, the torque is decreased (Fig. 8c) and the speed shows a slight overshoot that is quickly corrected to maintain a correct steady-state performance in no-load condition (Fig. 8a). In Test 4 the reference speed is changed from -300 to 300 rpm at $t = 10\ s$ in DVV-MPC and VV-MPC (left column and right column of Fig. 9 respectively). Both the current and speed tracking are satisfactory (Fig. 9a and 9b) and the phase currents invert the sequence in the zero-speed crossing (Fig. 9c). As a summary from tests 3 and 4, it can be observed that the dynamic performance of DVV-MPC is equal in practical terms to the one in VV-MPC. Therefore, the advantages in steady-state condition (shown in Test 1) are obtained with no impact on the dynamic performance.

Test 5 finally evaluates the steady-state response when the six-phase motor is driven at 700 rpm and 4.1 Nm (Fig. 10), showing the performance of VV-MPC (left plots) and DVV-MPC focused on α-β currents (right plots). While the motor speed is satisfactorily tracked in both techniques (Fig. 10a), the current control in d-q and x-y currents is improved (Fig. 10b and 10c) and this reduces in turn the distortion of phase currents (Fig. 10d). The THD of phase currents using DVV-MPC is 22.87% whereas VV-MPC provides a THD of 32.08%, hence the use of DVVs reduces the THD by 29% with the same parameters and operating conditions. This improvement in the current quality is in the same range as in test 1 (at 400 rpm with 3 Nm), where the THD improvement was quantified to be 33% (see table V).

To summarize, tests 1 and 5 quantify the significant improvements in the current quality at different steady-state conditions (Figs. 6 and 10), test 2 proves that the proposed DVVs increase the control flexibility (Fig. 7) and tests 3 and 4 confirm that the dynamic response of the proposed method is satisfactory (Figs. 8 and 9).

VI. Conclusions

MPC schemes are an interesting alternative for the control of multiphase machines thanks to their good dynamic response and high flexibility. However, standard MPC inevitably generates undesired x-y voltages because a single switching state is applied during the whole sampling period. Consequently, its performance can be highly degraded when the stator leakage inductance is low. This issue has been widely analyzed in the literature and several works have proposed the use of static virtual voltage vectors to mitigate this disadvantage. However, the solution provided by this approach presents some drawbacks from the point of view of the flexibility and voltage production. In order to outperform the MPC schemes based on static VVs, this work proposes the implementation of an MPC that includes dynamic virtual voltage vectors. The suggested DVVs provide MPC with a

higher flexibility and better current tracking because they are obtained online according to the operating point. Experimental results confirm that the proposed DVV-MPC achieves better current quality than VV-MPC, regaining at the same time a higher flexibility for the designer.

TABLE VI
TEST 2: PERFORMANCE QUALITY INDICES FOR DIFFERENT SETTINGS IN DVV-MPC

MPC version	THD_{ph} (%)	RMS_{ph} (A)	$THD_{\alpha\beta}$ (%)	σ_{xy} (A)
DVV-MPC focused on α-β currents	31.2	1.44	15.20	0.44
DVV-MPC focused on null voltage vector	30.9	1.38	14.07	0.41
DVV-MPC focused on medium voltage vectors	92.0	1.85	12.06	1.20

REFERENCES

[1] E. Levi, F. Barrero, and M. J. Duran, "Multiphase machines and drives—Revisited," *IEEE Trans. Ind. Electron.*, vol. 63, no. 1, pp. 429–432, Jan. 2016.

[2] F. Barrero and M. J. Duran, "Recent advances in the design, modeling, and control of multiphase machines—Part I," *IEEE Trans. Ind. Electron.*, vol. 63, no. 1, pp. 449–458, Jan. 2016.

[3] A. Tenconi, S. Rubino, and R. Bojoi, "Model Predictive Control for Multiphase Motor Drives – a Technology Status Review," *International Power Electronics Conference*, Niigata, Japan, 2018.

[4] P. F. C. Gonçalves, S. M. A. Cruz, and A. M. S. Mendes, "Comparison of model predictive control strategies for six-phase permanent magnet synchronous machines," *44th Annual Conference of the IEEE Industrial Electronics Society*, Washington DC, USA, 2018.

[5] E. Levi, R. Bojoi, F. Profumo, H.A. Toliyat and S. Williamson, "Multiphase induction motor drives- a technology status review," *IET Electric Power Application*, vol. 1, no. 4, pp. 489-516, 2017.

[6] E. Levi, "Advances in Converter Control and Innovative Exploitation of Additional Degrees of Freedom for Multiphase Machines," *IEEE Trans. Ind. Electron.*, vol. 63, no. 1, pp. 433-448, 2016.

[7] I. Gonzalez-Prieto, M.J. Duran, P. Entrambasaguas and M. Bermudez, "Field Oriented Control of Multiphase Drives with Passive Fault-Tolerance," *IEEE Trans. Ind. Electron.*, DOI. 10.1109/TIE.2019.2944056.

[8] L. Gao, J. E. Fletcher, and L. Zheng, "Low-speed control improvements for a two-level five-phase inverter-fed induction machine using classic direct torque control," *IEEE Trans. Ind. Electron.*, vol. 58, no. 7, pp. 2744–2754, Jul. 2011.

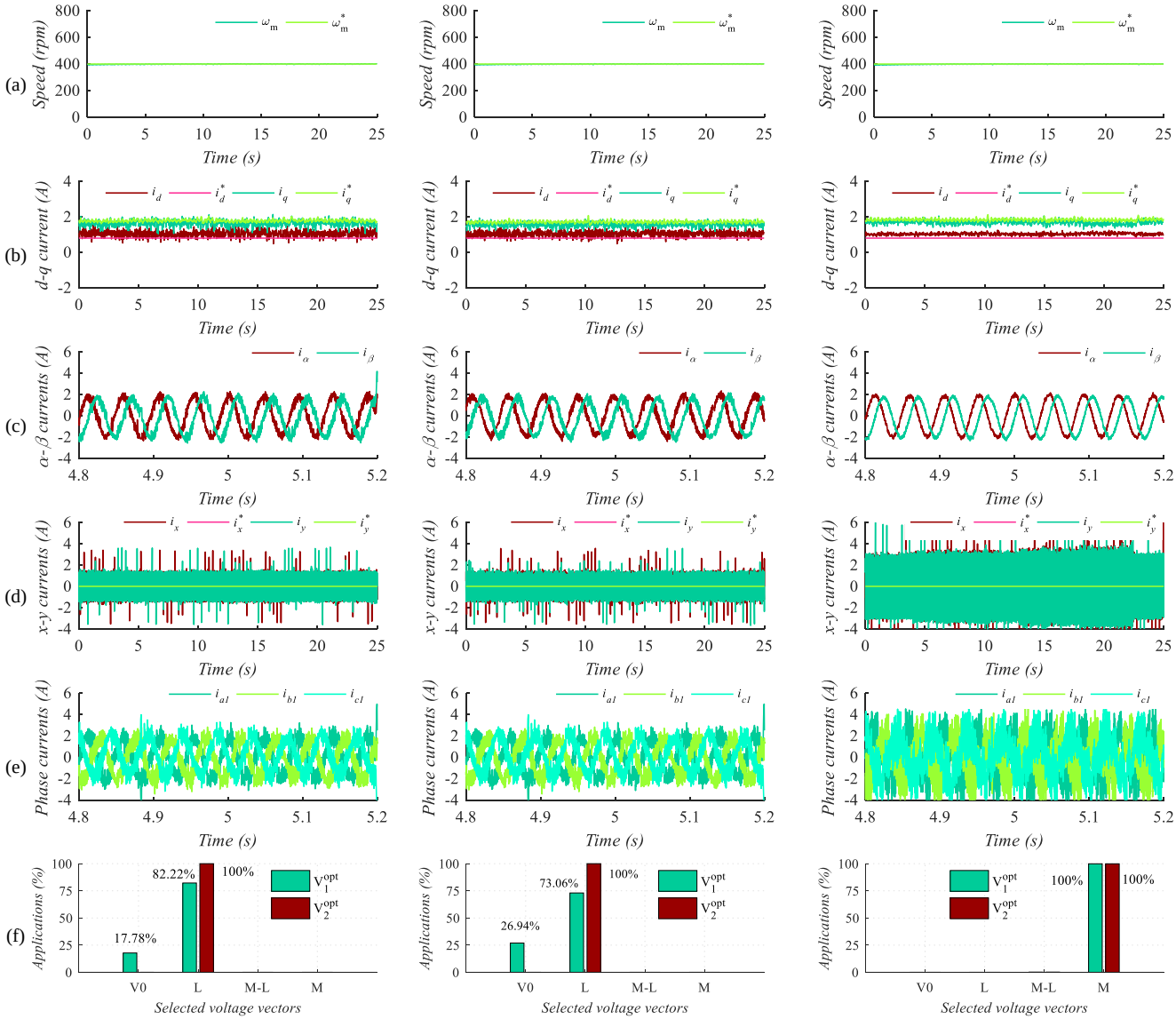

Fig. 7. Test 2: Steady-state performance of DVV-MPC focused on α-β currents (left column), DVV-MPC focused on null voltage vector (middle column) and DVV-MPC focused on medium voltage vectors (right column). From top to bottom: (a) motor speed, (b) d-q currents, (c) α-β currents, (d) x-y currents, (e) phase currents set#1 and (f) histogram of the selected voltage vectors.

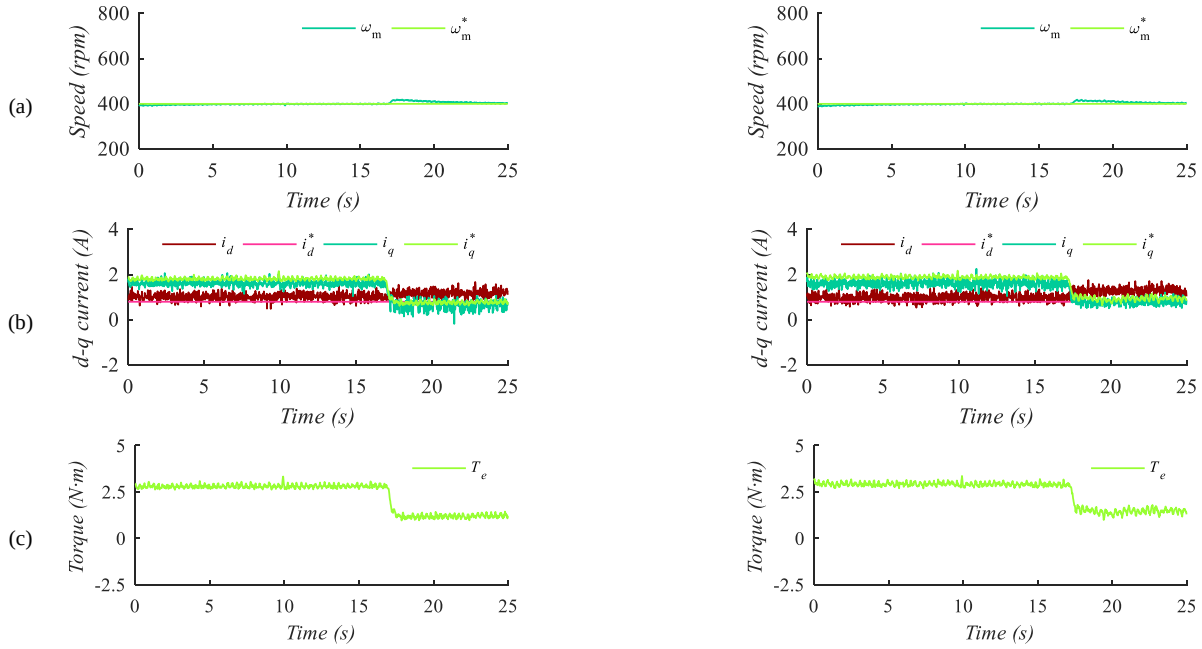

Fig. 8. Test 3: Dynamic response for change in load of DVV-MPC focused on α-β currents (left column) and VV-MPC (right column). From top to bottom: (a) motor speed, (b) d-q currents and (c) electromagnetic torque.

[9] DTC: A motor control technique for all seasons. ABB Group, Zurich, Switzerland.2015.[Online].Available:http://library.e.abb.com/public/0.e07ab6a2de30809c1257e2d0042db5e/ABB_WhitePaper_DTC_A4_20150414.pdf.

[10] S. Kouro, M. A. Perez, J. Rodriguez, A. M. Llor, and H. A. Young, "Model predictive control: MPC's role in the evolution of power electronics," *IEEE Ind. Electron. Mag.*, vol. 9, no. 4, pp. 8–21, Dec. 2015.

[11] F. Barrero, M. R. Arahal, R. Gregor, S. Toral, and M. J. Duran, "A proof of concept study of predictive current control for VSI-driven asymmetrical dual three-phase AC machines," *IEEE Trans. Ind. Electron.*, vol. 56, no. 6, pp. 1937–1954, Jun. 2009.

[12] M. J. Duran, E. Levi, and F. Barrero, "Multiphase electric drives: Introduction," in Proc. *Wiley Encyclopedia Electrical and Electronics Engineering*, pp. 1–26, Nov. 2017.

[13] F. Baneira, J. Doval-Gandoy, A. G. Yepes, Ó. López, and D. Pérez-Estévez, "Comparison of post-fault strategies for current reference generation for dual three-phase machines in terms of converter losses," *IEEE Trans. Power Electron.*, vol. 32, no. 11, pp. 8243–8246, 2017.

[14] A. González-Prieto, I. Gonzalez-Prieto, M. J. Duran and F. Barrero, "Efficient Model Predictive Control with Natural Fault-Tolerance in Asymmetrical Six-Phase Induction Machines," *Energies*, DOI. 10.3390/EN12203989.

[15] M. J. Duran, I. Gonzalez-Prieto, A. Gonzalez-Prieto, and F. Barrero, "Multiphase Energy Conversion Systems Connected to Microgrids With Unequal Power-Sharing Capability," *IEEE Trans. Energy Conv.*, vol. 32, no. 4, pp. 1386–1395, Dec. 2017.

[16] H. S. Che, E. Levi, M. Jones, M. J. Duran, W.-P. Hew, and N. A. Rahim, "Operation of a Six-Phase Induction Machine Using Series-Connected Machine-Side Converters," *IEEE Trans. Ind. Electron.*, vol. 61, no. 1, pp. 164–176, Jan. 2014.

[17] M. J. Duran, I. Gonzalez-Prieto, F. Barrero, E. Levi, L. Zarri, and M. Mengoni, "A Simple Braking Method for Six-Phase Induction Motor Drives With Unidirectional Power Flow in the Base-Speed Region," *IEEE Trans. Ind. Electron.*, vol. 64, no. 8, pp. 6032–6041, Aug. 2017.

[18] I. Subotic, N. Bodo, and E. Levi, "Single-Phase On-Board Integrated Battery Chargers for EVs Based on Multiphase Machines," *IEEE Trans. Power Electron.*, vol. 31, no. 9, pp. 6511–6523, Sept. 2016.

[19] L. Zheng, J. E. Fletcher, B. W. Williams, and X. He, "A novel direct torque control scheme for a sensorless five-phase induction motor drive," *IEEE Trans. Ind. Electron.*, vol. 58, no. 2, pp. 503–513, Feb. 2011.

[20] J. K. Pandit, M. V. Aware, R. V. Nemade, and E. Levi, "Direct torque control scheme for a six-phase induction motor with reduced torque ripple," *IEEE Trans. Power Electron.*, vol. 32, no. 9, pp. 7118–7129, Sep. 2017.

[21] J. K. Pandit, M. V. Aware, R. Nemade, and Y. Tatte, "Simplified implementation of synthetic vectors for DTC of asymmetric six-phase induction motor drives," *IEEE Trans. Ind. Appl.*, vol. 54, no. 3, pp. 2306–2318, May/Jun. 2018.

[22] Y. N. Tatte and M. V. Aware, "Torque Ripple and Harmonic Current Reduction in a Three-Level Inverter-Fed Direct-Torque-Controlled Five-Phase Induction Motor," *IEEE Trans. Ind. Electron.*, vol. 64, no. 7, pp. 5265–5275, Jul. 2017.

[23] Y. Ren and Z. Q. Zhu, "Enhancement of steady-state performance in direct-torque-controlled dual three-phase permanent-magnet synchro-nous machine drives with modified switching table," *IEEE Trans. Ind. Electron.*, vol. 62, no. 6, pp. 3338–3350, Jun. 2015.

[24] Y. Ren and Z. Q. Zhu, "Reduction of Both Harmonic Current and Torque Ripple for Dual Three-Phase Permanent-Magnet Synchronous Machine Using Modified Switching-Table-Based Direct Torque Control," *IEEE Trans. Ind. Electron.*, vol. 62, no.11, pp. 6671–668, Nov. 2015.

[25] C. Xue, W. Song, and X. Feng, "Finite control-set model predictive current control of five-phase permanent-magnet synchronous machine based on virtual voltage vectors," *IET Electric Power Appl.*, vol. 11, no. 5, pp. 836–846, May. 2017.

[26] C. Xue, W. Song, X. Wu, and X. Feng, "A constant switching frequency finite-control-set predictive current control scheme of a five-phase inverter with duty-ratio optimization," *IEEE Trans. Power Electron.*, vol. 33, no. 4, pp. 3583–3594, Apr. 2018.

[27] Y. Luo and C. Liu, "Multi-Vectors Based Model Predictive Torque Control for a Six-Phase PMSM Motor with Fixed Switching Frequency," *IEEE Trans. Energy Convers.* Early Access Article, 2019.

[28] B. Yu, W. Song, T. Tang, S. Wang, and P. Y. Bin, "A Finite Control Set Model Predictive Current Control Scheme for Five-phase PMSMs Based on Optimized Duty Ratio," *IEEE Applied Power Electronics Conference and Exposition*, Anaheim, USA, May 2019.

[29] P. F. C. Gonçalves, S. M. A. Cruz, and A. M. S. Mendes, "Fixed and Variable Amplitude Virtual Vectors for Model Predictive Control of Six-Phase PMSMs with Single Neutral Configuration," *IEEE International Conference on Industrial Technology*, Melbourne, Australia, Jul. 2019.

[30] P. F. C. Gonçalves, S. M. A. Cruz, and A. M. S. Mendes, "Predictive Current Control Based on Variable Amplitude Virtual Vectors for Six-Phase Permanent Magnet Synchronous Machines," *IEEE International Conference on Industrial Technology*, Melbourne, Australia, Jul. 2019.

[31] I. Gonzalez-Prieto, M. J. Duran, J. J. Aciego, C. Martin, and F. Barrero, "Model predictive control of six-phase induction motor drives using virtual voltage vectors," *IEEE Trans. Ind. Electron.*, vol. 65, no. 1, pp. 27–37, Jan. 2018.

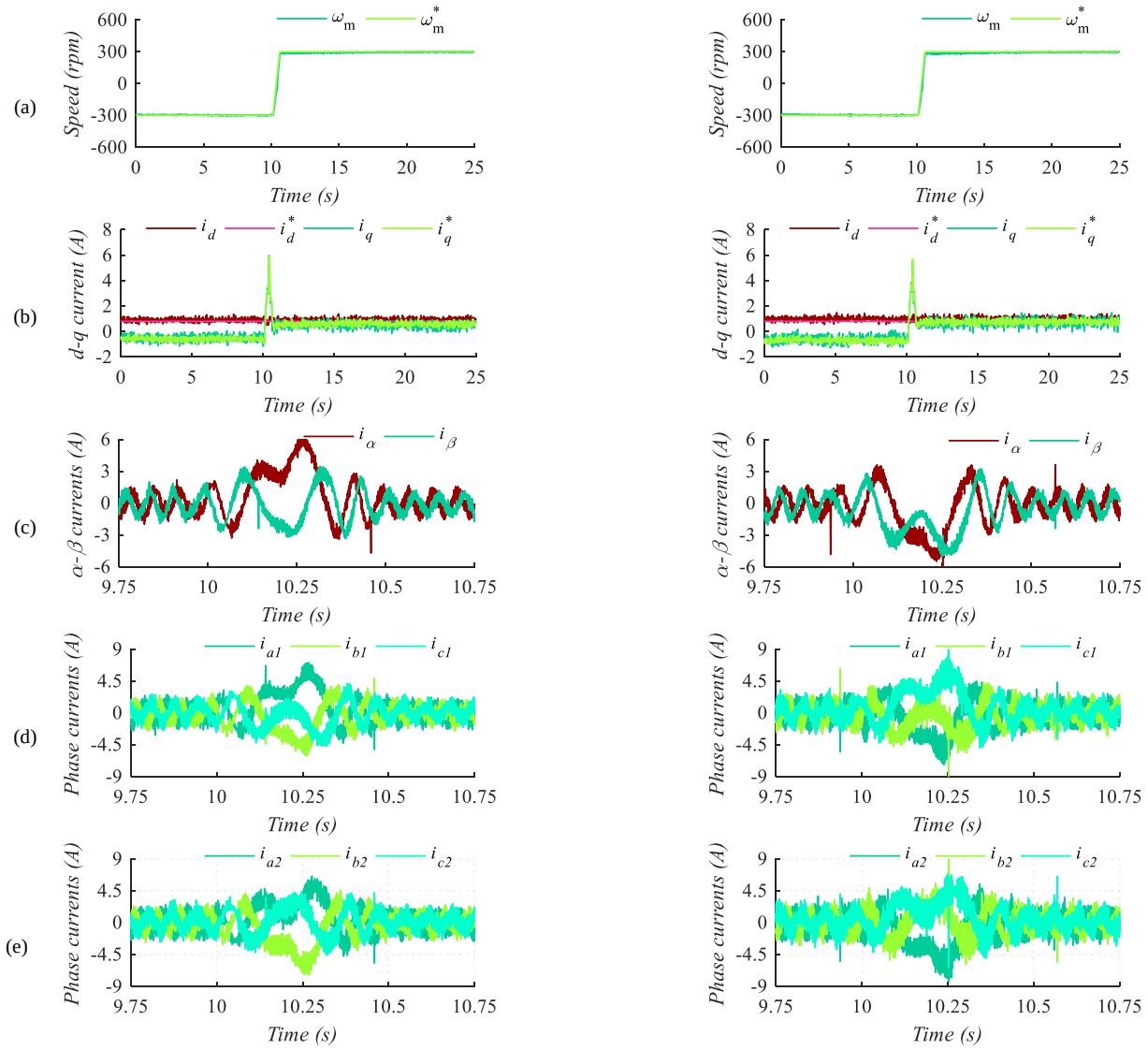

Fig. 9. Test 4: Speed reversal test for DVV-MPC focused on null voltage vector (left column) and VV-MPC (right column). From top to bottom: (a) motor speed, (b) d-q currents, (c) zoom of the α-β currents, (d) zoom of the phase currents set#1 and (e) zoom of the phase currents set #2.

[32] J. J. Aciego, I. Gonzalez-Prieto, and M. J. Duran, "Model predictive control of six-phase induction motor drives using two virtual voltage vectors," *IEEE J. Emerg. Sel. Topics Power Electron.*, vol. 7, no. 1, pp. 321–330, Mar. 2019.

[33] P. Garcia-Entrambasaguas, I. Zoric, I. Gonzalez-Prieto, M. J. Duran, and E. Levi, "Direct torque and predictive control strategies in nine-phase electric drives using virtual voltage vectors," *IEEE Trans.Power Electron.* Early Access Article. 2019.

[34] I. Gonzalez-Prieto, M. J. Duran, M. Bermudez, F. Barrero, and C. Martin, "Assessment of virtual-voltage-based model predictive controllers in six-phase drives under open-phase faults" *IEEE J. Emerg. Sel. Topics Power Electron.* Early Access Article. 2019.

[35] C. S. Lim, E. Levi, M. Jones, N. A. Rahim, and W. P. Hew, "FCS-MPC-Based current control of a five-phase induction motor and its comparison with PI-PWM control," *IEEE Trans. Ind. Electron.*, vol. 61, no. 1, pp. 149–163, Jan. 2014.

[36] M. R. Arahal, F. J. Barrero, M. J. Duran, M. G. Ortega, and C. Martin, "Trade-offs analysis in predictive current control of multi-phase induction machines," *Control Engineering Practice*, vol. 81, pp 105–113, 2018.

[37] E. Levi, "Multiphase electric machines for variable-speed applications," IEEE Trans. Ind. Electron., vol. 55, no. 5, pp. 1893–1909, May 2008.

[38] C. Martín, M. Bermúdez, F. Barrero, M. R. Arahal, X. Kestelyn, and M. J. Durán, "Sensitivity of predictive controllers to parameter variation in five-phase induction motor drives," *Control Engineering Practice*, vol. 68, pp. 23–31, Nov. 2017.

[39] A. G. Yepes, J. A. Riveros, J. Doval-Gandoy, F. J. Barrero, O. J. Lopez, B. Bogado, M. O. Jones, and E. Levi, "Parameter identification of multiphase induction machines with distributed windings—part 1: Sinusoidal excitation methods," *IEEE Trans. Energy Convers.*, vol. 27, no. 4, pp. 1056–1066, Dec. 2012.

[40] J. A. Riveros, A. G. Yepes, F. J. Barrero, J. Doval-Gandoy, B. Bogado, O. Lopez, M. Jones, and E. Levi, "Parameter identification of multiphase induction machines with distributed windings—part 2: Time-Domain techniques," *IEEE Trans. Energy Convers.*, vol. 27, no. 4, pp. 1067–1077, Dec. 2012.

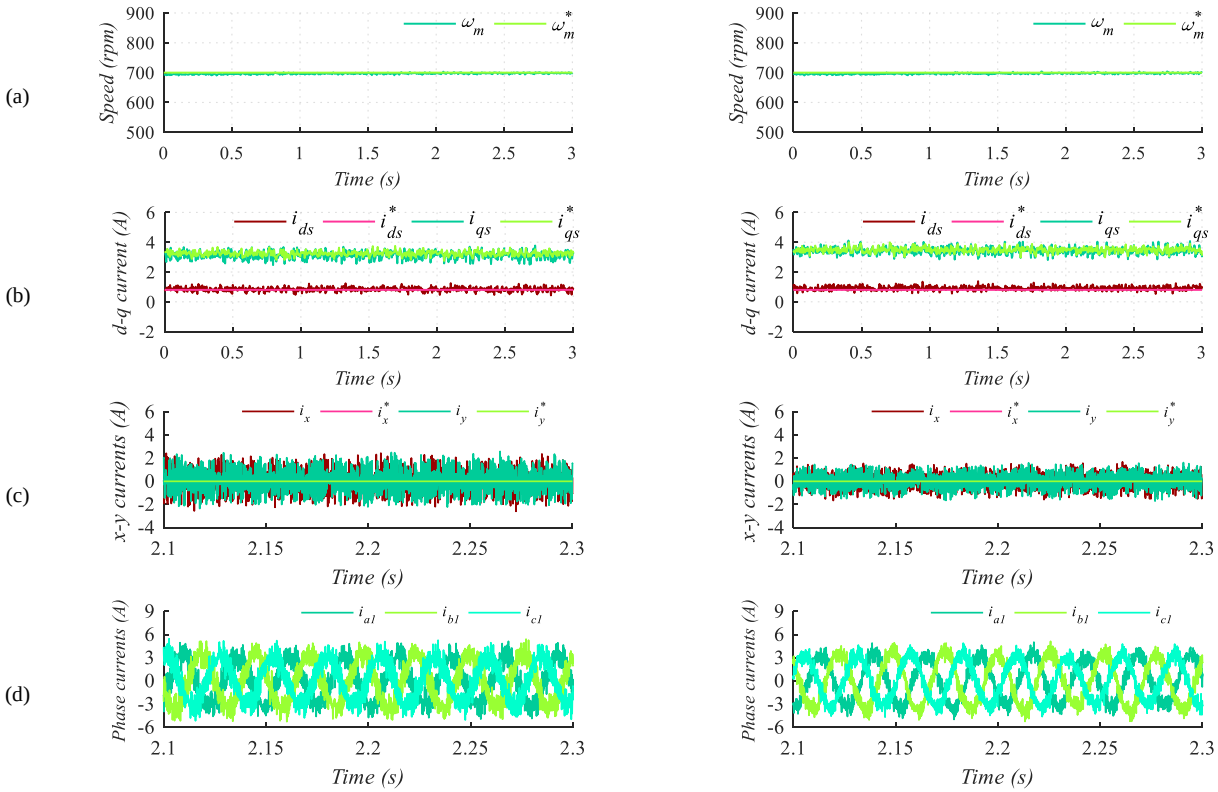

Fig. 10. Test 5: Steady-state performance of VV-MPC (left column) and DVV-MPC and DVV-MPC focused on α-β currents (right column). From top to bottom: (a) motor speed, (b) d-q currents, (c) x-y currents and (d) phase currents set#1.

Juan J. Aciego was born in Campillos, Spain, in 1976. He received the Industrial Engineering and M.Sc. degrees in mechanics and intelligent transport and energy systems from the University of Málaga, Málaga, in 2010 and 2016, respectively, where he is currently pursuing the Ph.D. degree with the Department of Electrical Engineering. His current research interests include power modeling and control of multiphase drives, renewable energy conversion systems, and electric vehicles.

Ignacio González Prieto was born in Málaga, Spain, in 1987. He received the Industrial Engineer and M.Sc. degrees in fluid mechanics from the University of Málaga, Málaga, Spain, in 2012 and 2013, ´ respectively, and the Ph.D. degree in electronic engineering from the University of Seville, Sevilla, Spain, in 2016. His research interests include multiphase machines, wind energy systems, and electrical vehicles

Mario J. Duran was born in Bilbao, Spain, in 1975. He received the M.Sc. and Ph.D. degrees in electrical engineering from the University of Málaga, Málaga, in 1999 and 2003, respectively. He is currently a Full Professor in the Department of Electrical Engineering, University of Málaga. His research interests include modeling and control of multiphase drives and renewable energies conversion systems.

Mario Bermudez was born in Málaga, Spain, in 1987. He received the B.Eng. degree in industrial engineering from the University of Málaga, Málaga, Spain, in 2014, and the Ph.D. degree in electrical/electronic engineering jointly from Arts et Métiers ParisTech, Lille, France, and from the University of Seville, Seville, Spain, in 2018. He is currently a Substitute Professor in the Department of Electrical Engineering, University of Huelva, Huelva, Spain. His research interests include modeling and control of multiphase drives, digital signal processor-based systems, and electrical vehicles.

Pedro Salas-Biedma was born in Fuengirola, Spain, in 1994. He received the B.Sc. degree in Industrial Engineering from the University of Málaga, Málaga, Spain, in 2017, where he is currently working toward the M.Sc. degree in Industrial Engineering. From 2018, he is a researcher in the Department of Electrical Engineering at the University of Málaga. His research interests include modelling and control of multiphase drives and renewable energy conversion systems.